Available online at www.sciencedirect.com
ScienceDirect
Journal of Magnetic Resonance 188 (2007) 151–159
JMR Journal of Magnetic Resonance
www.elsevier.com/locate/jmr

Unilateral MRI using a rastered projection

Christina L. Bray, Joseph P. Hornak *

Magnetic Resonance Laboratory, Center for Imaging Science, Rochester Institute of Technology, Rochester, NY 14623-5604, USA

Received 23 January 2007; revised 19 June 2007
Available online 4 July 2007

Abstract

Unilateral magnetic resonance techniques, where magnet and radio frequency (RF) coil are placed on one side of the sample, can provide valuable information about a sample which otherwise cannot be accommodated in conventional high spectral resolution magnetic resonance systems. A unilateral magnetic resonance imaging approach utilizing the stray field from a disc magnet and a butterfly geometry RF coil is described. The coil excites spins in a volume centered around an arc through the sample. Translating the RF coil relative to the magnet and recording the signal at each translational location creates a projection of the signal in a tomographic slice through the sample. Rotating the RF coil relative to the sample and repeating the translation creates projections through the sample at different angles. Backprojecting this information yields an image. A proof of concept device operating on this principle at 12.4 MHz was constructed and characterized. Projections through three phantoms are presented with a 1.2–4 cm field of view, thickness of 102 μm, and at a distance of 3 mm from the RF coil and 14 mm from the magnet. The edge spread function (ESF) was measured resulting in a 4 mm full width at half maximum (FWHM) line spread function (LSF) estimation using a Gaussian model. An example of one reconstructed image is presented.

Keywords: Unilateral MRI; Single sided MRI; Surface MRI; Instrumentation; Imaging; MRI; Backprojection reconstruction

1. Introduction

The majority of nuclear magnetic resonance experiments are performed in a mode where the source of the applied static magnetic field (B_o) and oscillating magnetic field (B_1) at the resonance frequency v are created with magnets and coils that surround, or are at least located on opposite sides of, the sample. Unilateral or single-sided magnetic resonance is performed by placing both the B_o and B_1 sources on the same side of the sample.

There are many potential applications of unilateral MRI, ranging from the macroscopic to the microscopic. On the macro scale, geophysical applications dominate. These include utility mapping, prospecting for aquifers, contaminant abatement, archeology, and earth dam assessment. An MRI based technique would compliment ground penetrating radar (GPR) which fails under conditions of high moisture and moderate conductivity where MRI should perform well. Moving towards microscopic dimensions, medical, food, and materials applications prevail. In food science, a unilateral system could be used for assessing moisture and oil content in foods and grains. In medicine, applications include dermatology, lymphology, and vascularity. In materials science, applications might range from studies of water in absorbing products, such as paper towels and diapers, to moisture ingress in organic light emitting diodes (OLED) and liquid crystal displays (LCD), to polymer rheology.

The terms unilateral and single-sided have been used in the literature to describe a variety of magnetic resonance systems [1–23]. We restrict our summary to include those systems where both B_o and B_1 magnetic fields are applied unilaterally. Therefore, stray-field (STRAFI) [16] and Gradient-At-Right-angles-to-Field (GARField) [17] NMR and MRI; and magnetic resonance sounding, NMR geotomography, and geophysical surface NMR [18–23] where either

* Corresponding author. Fax: +1 585 475 5988.
E-mail address: jphsch@rit.edu (J.P. Hornak).

1090-7807/$ - see front matter © 2007 Elsevier Inc. All rights reserved.
doi:10.1016/j.jmr.2007.06.010

the B_o or B_1 field is not applied unilaterally are not discussed.

Most examples of unilateral magnetic resonance from the literature detect a signal in the spatially decaying B_o field of a variety of permanent magnet geometries. Jackson developed the inside-out magnet geometry [2–4] for borehole logging [5,6]. Others have utilized a U-shaped, two-pole [7–9,15] or split U-shaped, four-pole [10,11] magnets where B_o is parallel to the surface of the probe. Paetzold et al., developed an NMR system pulled behind a tractor to detect soil moisture for remote sensing ground truth [15]. This system, a modified version of their earlier non-unilateral system [18], produced B_o parallel and B_1 perpendicular to the surface of the Earth. The unit detected an NMR signal as a function of depth by switching the resonance frequency of the RF coil. Blümich's laboratory developed the NMR mobile universal surface explorer (MOUSE) for probing relaxation times of materials a few mm beneath the surface [7]. Most versions of the NMR MOUSE also created a B_o field parallel to the surface of the probe and utilized an RF coil creating B_1 perpendicular to the surface [7,9,11]. One version of the MOUSE created B_o perpendicular and B_1 parallel to the surface [10]. Cylindrical [12] and concentric cylindrical [24,25] magnet geometries have also been employed which create a more homogeneous magnetic field region or *sweet spot* adjacent to the surface of the cylinder.

Many of these unilateral systems have been used to perform one-dimensional imaging by moving the coil, magnet, or both coil and magnet [8,11] relative to the sample; changing the resonant frequency of the RF coil [13,15]; or utilizing the gradient in the applied static B_o field [12]. Two-dimensional imaging has also been performed with phase and frequency encoding by applying pulsed field gradients in B_o [16].

Our approach [1] uses the stray field from a disk magnet and RF excitation from a butterfly shaped coil [26] to excite and detect a signal from spins located within a volume centered on a curved line through the sample. The B_o field is created perpendicular and B_1 parallel to the surface of the probe. Translating the coil along the face of the magnet allows generation of a projection of the signal in a curved tomographic slice above the magnet. Rotating the translation direction allows detection of projections at different angles and hence enabling the possibility of backprojecting the data to obtain an image. This design has several self-apodizing aspects that restrict signal detection to spins located above the magnet.

2. Background

Consider a disk shaped rare-earth permanent magnet with north and south poles of the magnet on opposite faces of the disk. (See Fig. 1a.) Define the standard magnetic resonance coordinate system relative to the magnet with the Z axis perpendicular to the face. In this arrangement, B_o is parallel to Z at $(x, y) = 0, 0$ and makes an acute angle with

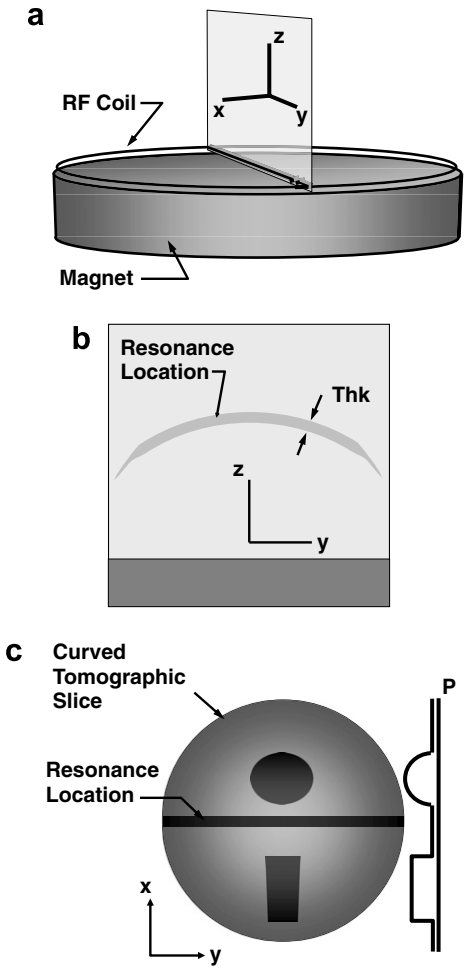

Fig. 1. Schematic representations of the (a) apparatus showing the magnet and RF coil with respect to the standard magnetic resonance coordinate system, (b) resonance location of thickness Thk in the ZY plane above the magnet, and (c) projection (P) of the signal in the resonance location as the RF coil is moved along X.

the normal to the surface as the distance from $(x, y) = 0, 0$ increases. Because the B_o field drops off with distance Z from the magnet, a thin curved resonance surface exists above the face of the magnet where spins experiencing a frequency ν will resonate. For a spread of frequencies $\Delta\nu$ centered on ν, the resonance condition will be met in a curved tomographic slice above the face of the magnet with thickness (Thk) determined by the drop off in B_o with distance from the magnet.

A butterfly shaped RF coil, shown schematically in Fig. 1a, resonant at ν is placed on the surface of the magnet such that its center inductor lies along the Y axis. In any one half of an RF cycle, current flows through the center inductor and around the two wings or outer loops in opposite directions. This resonance pattern creates an RF magnetic field that comes out of the center of one wing, around the center inductor, and into the center of the opposite wing. The coil produces B_1 RF fields with components parallel to Z in the center of the D-shaped halves, and perpendicular to Z above the inductors. Focusing on the region

above the center inductor of the coil where B_1 is perpendicular to B_o, we see there is an area centered around an arc through the curved tomographic resonance slice where spins may be excited and a signal detected. (See Fig. 1b.) Several factors minimize the contribution to an NMR signal from spins above the remainder of the inductor. These include the relative diameter of the magnet and butterfly coil, the size of the sample, and the diminished B_1 field above the outer portions of the inductor.

When using a 90° pulse sequence, the NMR signal (S) for a given volume element is proportional to the cross-product between the equilibrium magnetization ($\vec{M}_0$) and $\vec{B}_1$ vectors. The total signal from a sample smaller than the diameter of and centered on the butterfly coil is proportional to the sum of signals from all voxels in the resonance region above the magnet defined by coordinates (x, y, z).

$$S \propto \int\int\int \vec{M}_0(x,y,z) \times \vec{B}_1(x,y,z)\,\mathrm{d}x\,\mathrm{d}y\,\mathrm{d}z \tag{1}$$

Only components of $\vec{B}_1 \perp \vec{M}_0$ contribute to the signal. In the butterfly coil, this coincides with the regions above the inductor. Because the current in an outer loop of the butterfly coil is half the current in the center inductor, the signal is primarily from spins above the center inductor of the coil. This can be further constrained by designing the size of the sample to be less than the radius of the butterfly coil as depicted in Fig. 1a, or by making the radius of the butterfly coil equal to at least the diameter of the magnet. The thickness of the tomographic slice where resonance can occur is determined by the bandwidth of the RF excitation pulse(s) and the gradient in B_o. Decreasing the amplitude of an RF excitation pulse, and increasing its length, decreases the signal because the slice thickness is reduced. Moreover, increasing the amplitude of an RF excitation pulse and decreasing the pulse length, increases the slice thickness. Therefore the NMR signal has contributions primarily from a region of thickness Thk above the center inductor.

The X location of the RF coil can be varied relative to the position of the magnet to change the location of the arc through the curved tomographic slice. The area under the NMR signal as a function of the X location of the RF coil represents the projection of this signal from within the resonance location onto the projection axis (P) or X-axis in this case. (See Fig. 1c.) Varying the orientation of the RF coil in the XY-plane will produce projections at angles ϕ about Z. This imaging is similar to projection imaging [27] with the following exceptions. First, the imaged tomographic slice is curved rather than planar. Second, the tomographic slice thins towards the edge of the slice due to an increase in the gradient near the edge of the disk magnet. Third, the projection intensity at any P value is the sum of signal from a volume defined by Thk and the width of the region where $\vec{B}_1 \perp \vec{M}_0$.

There are some limiting assumptions associated with this technique. Ideal backprojection imaging will only be possible in two general cases. The first is when a disk shaped magnet is used and its diameter is less than or equal to the radius of the butterfly coil. In this case, the maximum field of view (FOV) may never exceed the dimensions of the tomographic resonance slice above the magnet. The second is when the largest dimension of the imaged object is less than the radius of the butterfly coil which in turn is smaller than the planar magnet of any shape. In this second case, the maximum FOV is approximately equal to the radius of the butterfly coil.

Reconstruction of the image involves warping the result of the inverse Radon transform onto an appropriate curved surface. Imaging of the volume above the magnet can be achieved by acquiring a signal from a series of concentric curved planes, achieved by the mechanical approach of varying the distance between the RF coil and magnet [11], or by the electrical approach of changing the coil tuning and ν_o [13,15,18].

3. System design and characterization

Our proof of concept system consisted of a magnet, RF coil, and a Bruker DRX-300 liquids NMR spectrometer. The spectrometer served as the pulse programmer, source of RF power, RF detector, and digitizer. This liquids spectrometer provided up to 100 W of RF power down to ~10 MHz and quadrature digitization at 286 kHz. Post processing of the data was performed using Matlab (The Mathworks, Natick, MA) and IDL (ITT Visual Information Solutions, Boulder, CO).

The specific form of the butterfly coil chosen for the proof of concept system was the result of an iterative process. To minimize the required capacitance and to concentrate the B_1 field above the center inductor, the basic butterfly coil design of Fig. 1a was modified to that depicted in Fig. 2. Multiple turns wound similar to a *figure-8* coil were used instead of a single loop. The outer

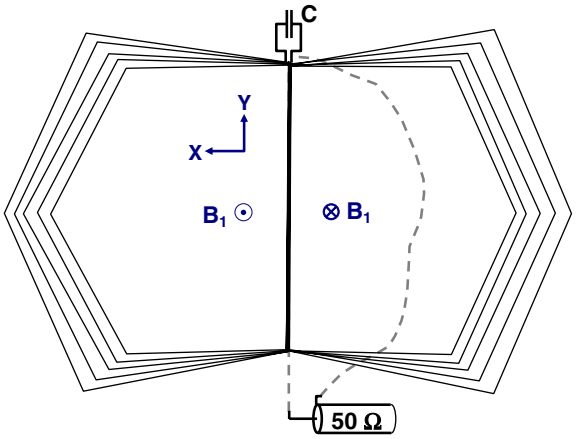

Fig. 2. A schematic representation of the multi-turn butterfly coil with its 4 cm long center inductor and 7 cm diameter. Solid lines indicate the location of the windings of the continuous inductor which overlap in the center and terminate at capacitor C. Dashed line is the location of the inductive coupling loop which is connected to a 50 Ω transmission line. The ⊙ and ⊗ symbols represent the relative B_1 field directions in the XY plane.

windings were also spread out in the XY plane. This design was chosen because it should decrease B_1 above the outer inductors relative to the center inductors. A total of five turns of #30 enameled copper wire were used in each wing for a total of 10 inductors in the center. The smaller diameter inductor was chosen to minimize the thickness of the multi-turn coil. The length of the center inductor portion of the multi-wing style was 4 cm. The coils were mounted on a 7.3 cm diameter, 2 mm thick Teflon form. The form was mounted within a PVC frame with a copper ground plane located between the magnets and the RF coil. The ground plane made the resonant frequency of the coil insensitive to translational motion across the magnet. The presence of the ground plane also increased the coil quality factor (Q).

The coil was tuned to a nominal resonance frequency of 12.4 MHz using fixed high voltage non-magnetic capacitors (Centralab) with a total capacitance of 45 pF. The coil was inductively coupled with a single D-shaped loop of #26 enameled copper wire placed over a portion of one wing of the butterfly coil. The coil had a Q of 25.

The B_{1x} magnetic field in the YZ and XZ planes above the multiple wing butterfly RF coil was measured on a 2.5 mm grid using a 1 mm diameter, 2 mm length, 10 turn pickup coil of #36 copper wire and an oscilloscope [28]. Additional measurements were collected off the grid to characterize null points where B_{1x} changed directions. Contour plots of B_{1x} are presented in Fig. 3. The B_{1x} field values are relative to the maximum value measured near the center inductor. The B_{1x} field contours in the YZ plane near the surface of the coil are almost flat and closely match the gentle curvature in the B_o field contours. (See Fig. 3a.) This shape facilitates equal rotation angles along the resonance arc through the curved tomographic slice. In the XZ-plane data presented in Fig. 3b, the B_{1x} field was five times greater above the center inductor than the inductors at the outer wings. This characteristic helps concentrate the signal from above the center inductor while minimizing signal contributions from the outer edges in X of the butterfly coil.

The magnet on our apparatus consisted of a stack of four 7.62 cm diameter by 1.27 cm thick disk NdFeB magnets (Scientifics, Tonawanda, NY) with north and south poles located on opposite faces of a disk. With this magnet geometry, field lines emanate from a flat face of the end disk and loop around to the face on the opposite end disk. Magnetic field simulations (Maxwell 2D, Ansoft Corp., Pittsburgh, PA) show that the multiple-disk configuration pushes the magnetic field contours further from the faces of the end disks and lessens the rounding of the contours near the edges of the disk faces. We arbitrarily stopped at a four disk stack of magnets because the gain in desirable field characteristics diminished with each disk added.

The magnitude and direction of the B_o magnetic field above the stack of magnets was measured in the YZ plane on a 0.5 cm grid using a Hall probe Gauss meter (Applied Magnetics Laboratory, Baltimore, MD). The field as a function of distance Z from the disk decreased from a high value of 0.5 T near the face of the end disks. B_o contour lines, shown in Fig. 4, have a slight curvature extending further from the center of the disk than the edges causing the resonance location adjacent to the magnet to possess

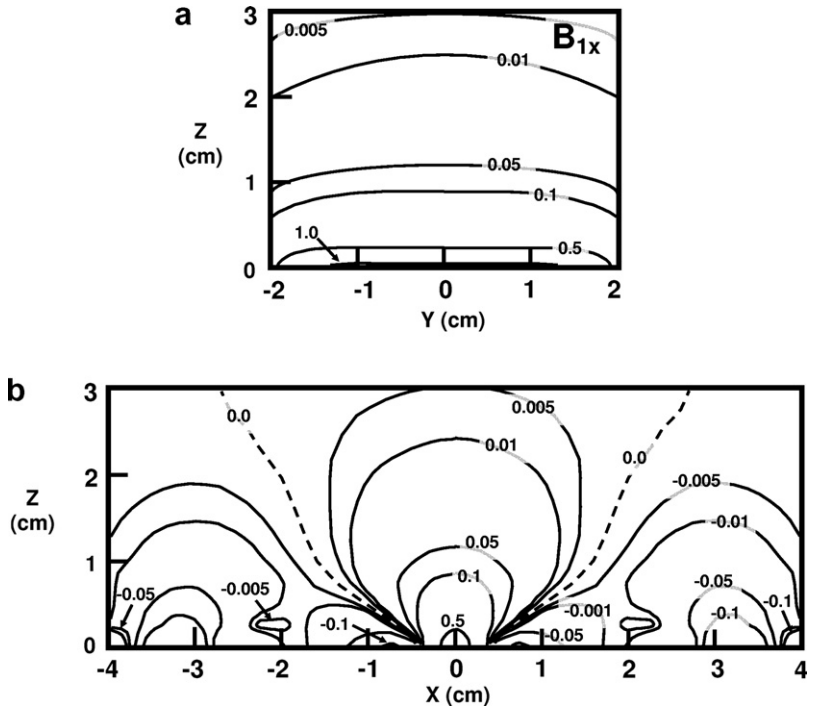

Fig. 3. The x component of the measured B_1 magnetic field in the (a) YZ- and (b) XZ-planes above the RF coil. B_{1x} values are relative to the maximum measured value in the plane.

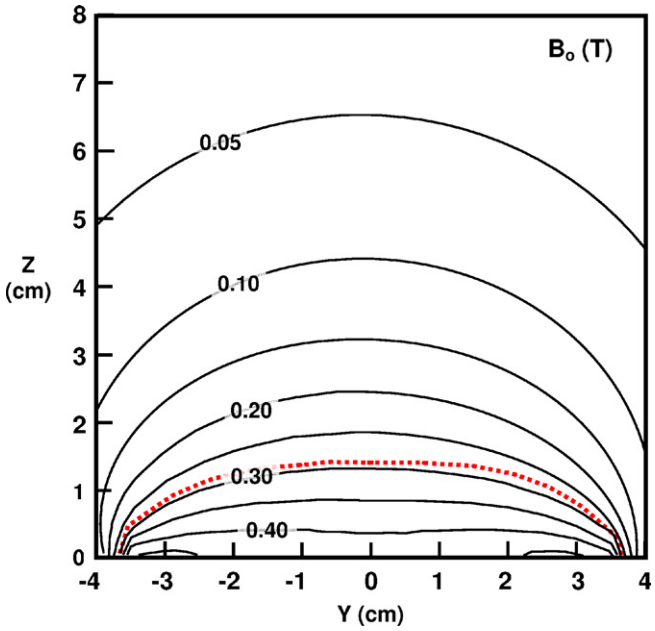

Fig. 4. Contour plot of the measured B_o magnetic fields in Tesla for the YZ-plane above the disk magnets. Resonance location at 12.4 MHz is depicted by the dashed line.

a similar curvature. The resonance location for protons at 12.4 MHz is depicted as the dashed line in Fig. 4.

The magnet stack, butterfly coil, and sample were located inside a 20 cm diameter, 30 cm length Faraday shield to minimize environmental noise. (See Fig. 5.) The magnet was stationary in X and Y at the center bottom of the Faraday cage. The magnet could be moved in Z to shorten or lengthen the distance between the face of the magnet and the RF coil, thus changing the position of the tomographic resonance slice relative to the RF coil. In our embodiment, we chose to move the butterfly coil in the X direction across the face of the magnet with a worm-gear assembly. The sample was positioned over the center of the magnet on an arm that allowed it to be rotated about its axis by ϕ. The combination of translation and rotation allowed realization of the rastered projections.

Petroleum jelly filled Teflon phantoms, denoted as phantoms a–c in Fig. 6, were imaged to determine spatial resolution of the technique. All Teflon containers had a 3.8 cm OD which fit into the rotation arm of the Faraday cage. The geometries of the petroleum jelly filled voids within the phantoms were: (a) a 2.9 cm ID circular cylinder with a circular cylindrical 1.0 cm diameter zero signal Teflon plug, (b) two 1.3 cm ID circular cylinders separated on center by 1.7 cm, (c) an offset 1.5×2.0 cm rectangular cylinder. All phantoms were imaged such that the axis of the cylinder was parallel to Z. In the axially asymmetric phantoms, ϕ defines the projection angle through the phantom.

A Hahn spin-echo sequence [29] was used to record the NMR signal from the resonance location of Fig. 1b. This sequence was required because of the extremely short T_2^* associated the spins in an inhomogeneous magnetic field and the difficulty digitizing close to the end of an RF pulse.

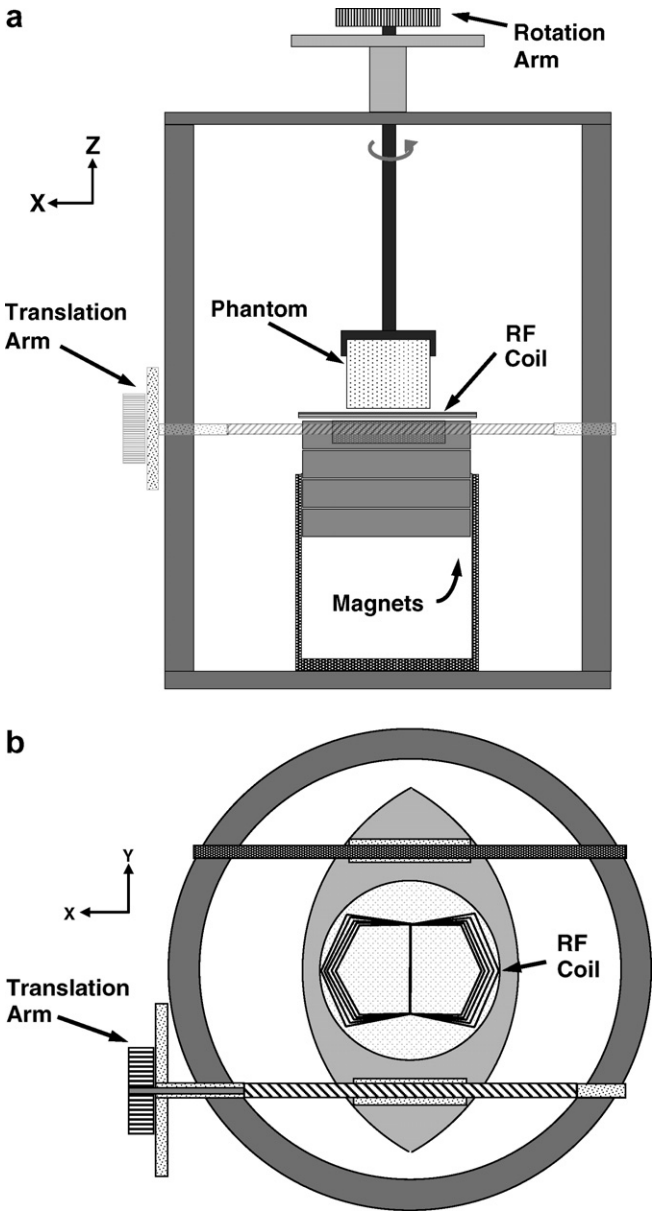

Fig. 5. Cross-sectional views of (a) vertical and (b) horizontal planes through the non-magnetic shielding apparatus used to rotate the phantom and translate the RF coil relative to the magnet.

A 2 ms echo time, 1 s repetition time sequence with 512 averages, 128 complex points, 3.35 μs dwell time, and 50 μs width Gaussian 90° and 180° pulses were used to record a full echo from the sample. Echoes were recorded at various positions of the coil along its translational direction X for various orientations of the phantoms at rotation angles ϕ about Z. Although changing the resonance frequency of the coil will change the slice location relative to the surface of the RF coil, the resonance frequency was held constant in all experiments. Instead the distance between the magnet and RF coil was varied to change the slice location. Projections through the phantoms were taken at increments of ϕ, and all at a height of 3 mm above the RF coil and 14 mm from the magnet. Owing to the

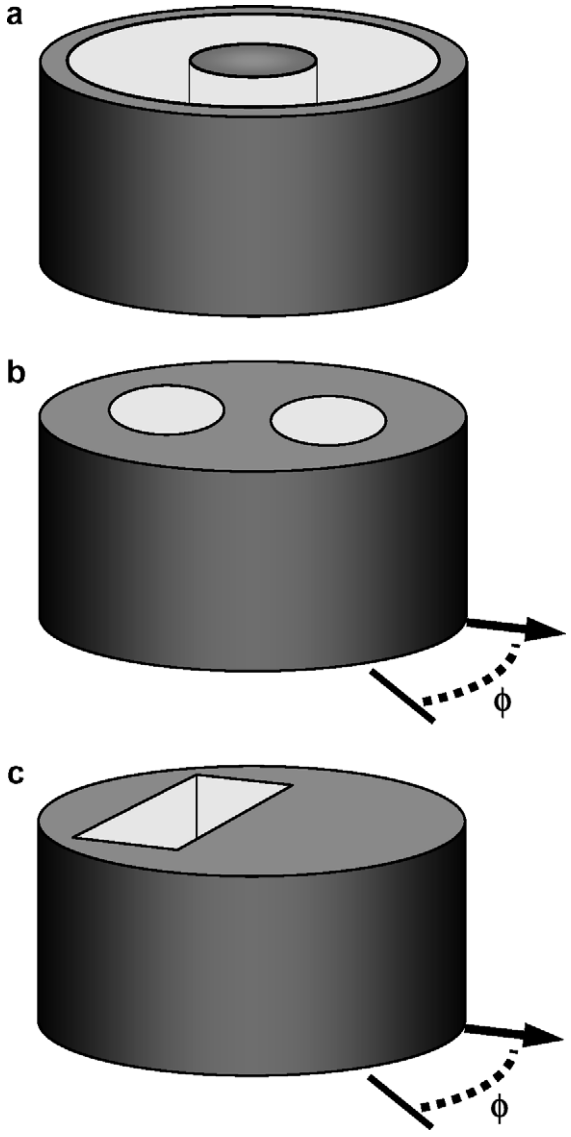

Fig. 6. The petroleum jelly filled (a) cylinder with a cylindrical zero-signal plug, (b) two cylinder, and (c) edge spread function Teflon phantoms.

central ordinate theorem [30], the NMR signal was taken as the echo magnitude smoothed with a five-point triangular function to improve peak estimation.

4. Results and discussion

The thickness of the curved tomographic slice thins as the distance r from the Z axis increases. Based on the measured B_o gradient and the FWHM frequency content of a 50 μs Gaussian 12.4 MHz RF pulse being 17.65 kHz, the slice thickness can be determined as a function of r. When $r \leqslant 2.25$ cm Thk = 102 μm ±10%. Thk drops off rapidly to 23 μm by $r = 2.75$ cm and 9 μm by $r = 3.75$ cm, thus, serving to limit the sensitivity in this resonance tomographic slice to $r \leqslant 2.25$ cm. The thinning of Thk as r increases is depicted in Fig. 1b. This is significant because the B_o gradient plays a major role in apodizing the signal.

As the chosen resonance frequency of the coil decreases, the location of the curved tomographic slice moves further away from the coil. The amount of RF power necessary to produce the desired rotations in a pulse sequence increases and the signal-to-noise ratio (SNR) decreases. A SNR of eight was obtained for phantom a at $P = 0$ with an ensemble average consisting of 512 scans. Signal could be recorded at greater distances from the coil, but with more averages and a larger acquisition time.

Projections of the NMR signal in the curved tomographic slice through the phantoms yielded the expected profiles. Fig. 7 is a projection through phantom a using the butterfly coil and consists of 32 points along a 4 cm P axis. The data points show discernable agreement with the predicted signal in the tomographic resonance plane, depicted in Fig. 7 by the dashed line.

The second and more complex phantom imaged is phantom b, the two circular-cylinder phantom. Projections through this phantom were taken at $\phi = 0°$, 30°, 60°, and 90°, as defined in Fig. 6, using 31 points in 3 cm along P. All projection angles presented in Fig. 8 show discernable agreement with the predicted projection signal depicted by the dashed line.

Although a sufficient number of projections were not taken to create a quality tomographic image, the four projections through phantom b were used simply to demonstrate the concept of producing a tomographic image. The inverse radon transform was applied to the projections in Fig. 8 without the digital filtering routinely applied in a backprojection [31]. For comparison, the theoretical projections were also backprojected with the same sampling resolution and at the same angles. Fig. 9 presents these projections with identical brightness and contrast settings. Two high-signal regions are visible in each image. The oval-shape of the regions is primarily due to the lack of symmetry in the projection angles due to missing projections at 120° and 150°.

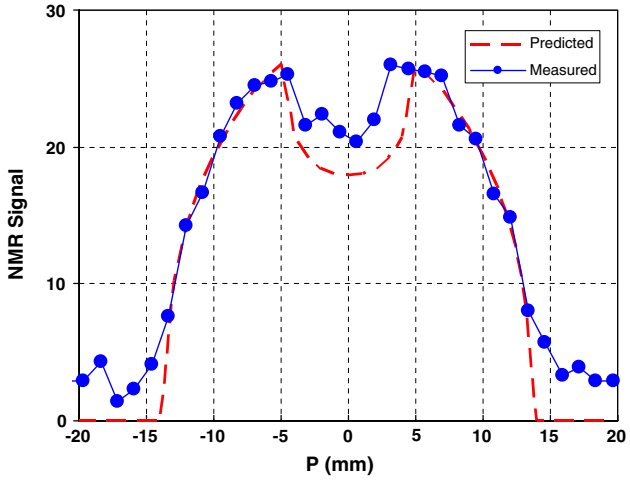

Fig. 7. Experimental (●) and theoretical (---) projections through phantom a.

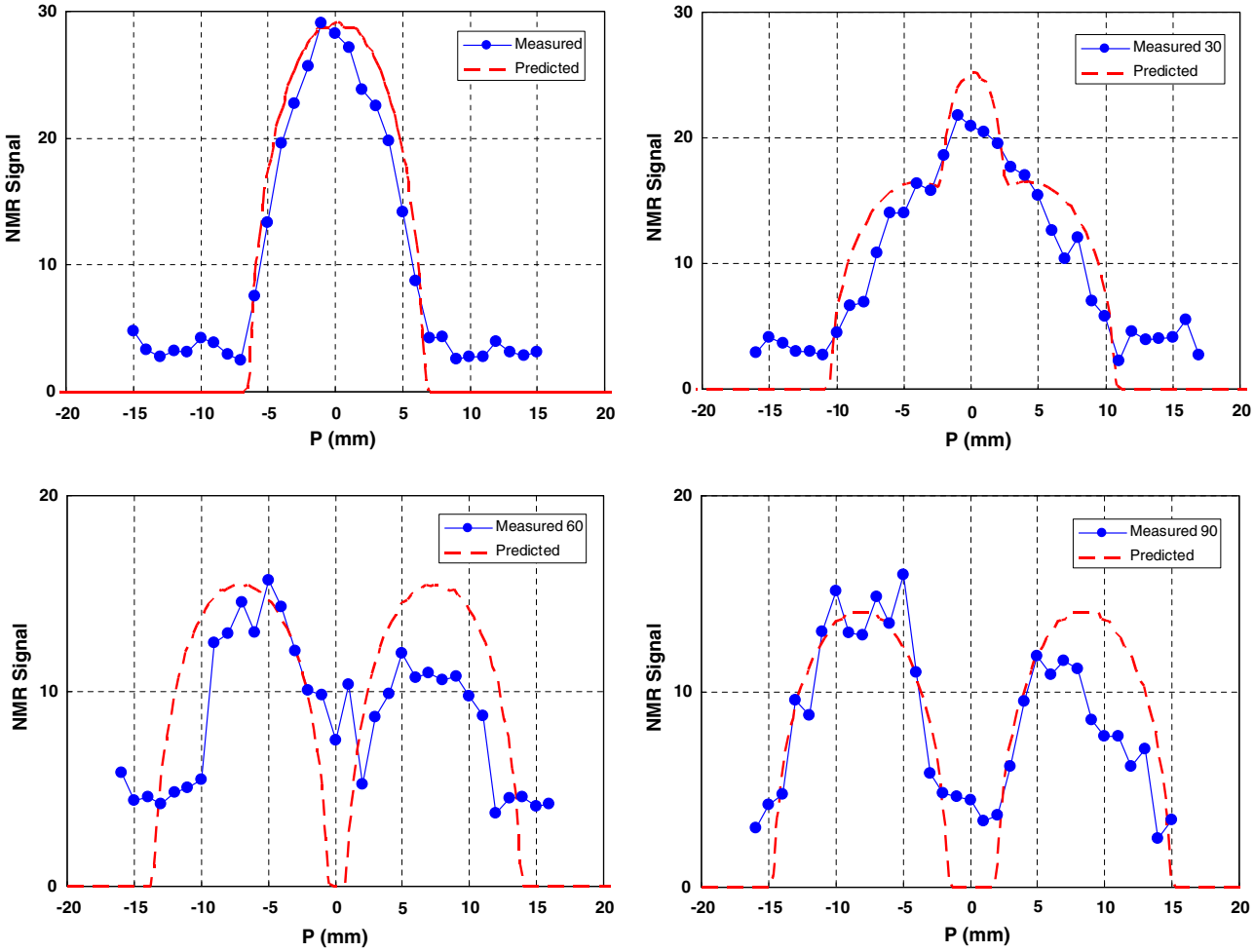

Fig. 8. Experimental (●) and theoretical (---) projection data for phantom b at $\phi = 0°$, 30°, 60°, and 90°.

The third phantom, phantom c, was used to determine the line spread function for the imaging system. Two projections through this phantom along P at $\phi = 0$ with a density of 18 points in 11 mm are presented in Fig. 10. Various width Gaussian shaped functions were convolved with a theoretical edge or step function [30] to produce a best-fit model of the measured edge spread function data. The convolution of a Gaussian function with a FWHM of 4 mm gave the best fit to the edge profile seen in Fig. 10. Therefore, the projection resolution of our system is 4 mm at 3 mm from the coil and 14 mm from the magnet. The resolution should improve as distance from the magnet decreases because the width of a B_{1x} contour decreases as Z decreases.

Agreement between the measured and predicted projections through all phantoms is currently limited by the 4 mm resolution of the system, provided the projection step size is less than 4 mm, and the signal-to-noise ratio of the NMR data. The SNR is limited by Thk. Higher power, narrower RF pulses with a frequency content less than the bandwidth of the butterfly coil will be needed to increase Thk. The SNR is also expected to decrease as Z increases.

5. Conclusions

Our results demonstrate the rastered projection approach to unilateral MRI. The unilateral system with its 7.6 cm diameter magnet and 7 cm diameter butterfly coil can produce 102 μm Thk projections with 4 mm resolution at a distance of 3 mm from the RF coil and 14 mm from the magnet. Poorer resolution will be seen as distance from the RF coil increases.

Currently, the available RF power from the host NMR spectrometer limits both the imaging depth and SNR. Because B_1 drops off with distance from the RF coil, more power is needed to image at greater distances. Increasing the pulse width will not help because this diminishes the frequency content or range of the RF pulse and hence the slice thickness. Ideally, shorter, higher power RF pulses, which can easily be accommodated by the bandwidth of the RF coil, are needed to increase the slice thickness and thus improve SNR. An improved SNR will allow shorter acquisition times per projection point. An additional way to decrease the acquisition time and maintain the SNR is by averaging the echoes from a

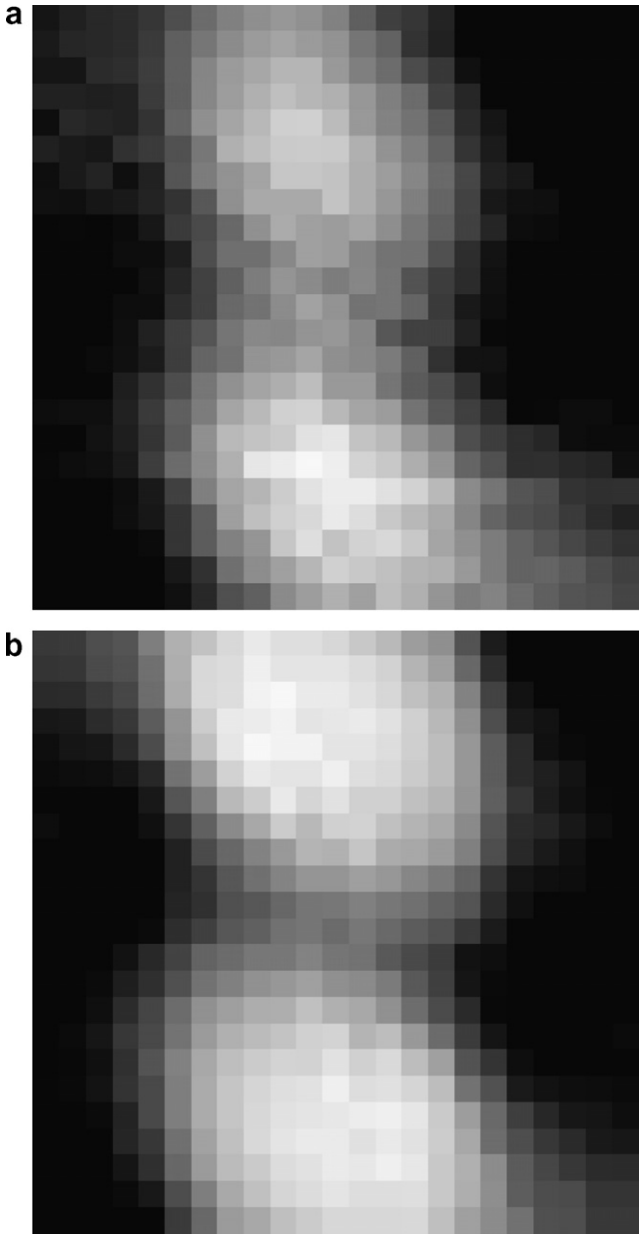

Fig. 9. A projection image of phantom b from the four (a) experimental and (b) theoretical projections presented in Fig. 8. Brightness and contrast settings, and the number of projection points, are identical for the two images.

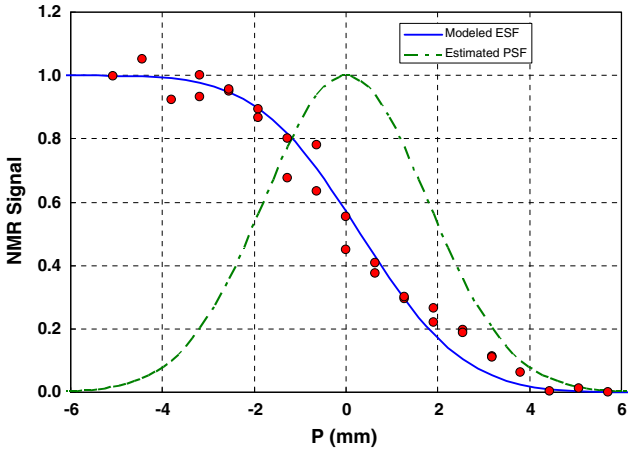

Fig. 10. Measured (●) NMR signal as a function of distance P in mm perpendicular to the void edge in phantom c. Modeled NMR signal (——) is based on a Gaussian line spread function (– – –).

Carr–Purcell–Meiboom–Gill [32,33] sequence rather than a Hahn echo sequence.

In-plane resolution is presently limited by the characteristics of the B_o and B_1 field distributions. In general, the resolution performance should improve as the distance from the coil decreases. To improve overall resolution it will be necessary to modify either B_o or B_1 such that the locations where the B_1 field is perpendicular to B_o is smaller than in the current design. One method might be to bring the outer loops of the butterfly coil closer to the center loop, thus compressing Fig. 3b in X. This however introduces signal from outer loops which could be removed via a deconvolution technique [34] or by further reducing the B_o homogeneity over the outer loops using surface spoiling [35,36]. To achieve a projection resolution of 0.4 mm will require a reduction in the width of the region above the RF coil where $\vec{B}_1 \perp \vec{M}_0$ by a factor of 10.

The rastered projection MRI approach should be scaleable to larger systems to image larger FOVs at correspondingly larger distances from the coil. However, safety issues related to large permanent magnets will need to be addressed.

Acknowledgments

We thank S. Iannopollo for assistance with the field measurements, T. Lucero and A. Bright for assistance with projection data collection, J. Bodie for computer support, and S. Kaplan and A. Klymachyov for helpful discussions.

References

[1] C.L. Bray, S. Iannopollo, J.P. Hornak, Design and Characterization of a Sub-Surface MRI System, 15th Triennial Conference for the International Society for Magnetic Resonance, Ponte Verda Beach, FL, October 2004.
[2] R.K. Cooper, J.A. Jackson, Remote (inside-out) NMR.I. Remote production of a region of homogeneous magnetic field, J. Magn. Reson. 41 (1980) 400–405.
[3] L.J. Burnett, J.A. Jackson, Remote (inside-out) NMR. II. Sensitivity of NMR detection for external samples, J. Magn. Reson. 41 (1980) 406–410.
[4] J.A. Jackson, L.J. Burnett, J.F. Harmon, Remote (inside-out) NMR. III. Detection of nuclear magnetic resonance in a remotely produced region of homogeneous magnetic field, J. Magn. Reson. 41 (1980) 411–421.
[5] K.J. Dunn, D.J. Bergman, G.A. LaTorraca, Nuclear Magnetic Resonance Petrophysical and Logging Applications, Pergamon, Amsterdam, 2002.
[6] R.L. Kleinberg, J.A. Jackson, An introduction to the history of NMR well logging, Concepts Magn. Reson. 13 (2001) 340–342.
[7] G. Eidmann, R. Savelsberg, P. Blümler, B. Blümich, The NMR Mouse, a mobile Universal Surface Explorer, J. Magn. Reson. A122 (1996) 104–109.

[8] J.C. Edwards, NMR Surface Sensors, Process NMR Associates, Danbury, CT, 2006, http://www.process-nmr.com/nmr_surface_sensors.htm.
[9] G. LeBec, J.P. Yonnet, K. Raoof, Coil and Magnet design for nuclear magnetic resonance in inhomogeneous field, IEEE Trans. Magnetics 42 (2006) 3861–3867.
[10] F. Casanova, B. Blümich, Two-dimensional imaging with a single-sided NMR probe, J. Magn. Reson. 163 (2003) 38–45.
[11] J. Perlo, F. Casanova, B. Blümich, Profiles with microscopic resolution by single-sided NMR, J. Magn. Reson. 176 (2005) 64–70.
[12] S. Rahmatallah, Y. Li, H.C. Seton, I.S. Mackenzie, J.S. Gregory, R.M. Aspden, NMR detection and one-dimensional imaging using the inhomogeneous magnetic field of a portable single-sided magnet, J. Magn. Reson. 173 (2005) 23–28.
[13] P.J. Prado, Single sided imaging sensor, Magn. Reson. Imag. 21 (2003) 397–400.
[14] P.J. Prado, NMR hand-held moisture sensor, Magn. Reson. Imag. 19 (2001) 505–508.
[15] R.F. Paetzold, A. De Los Santos, G.A. Matzkanin, Pulsed nuclear magnetic resonance instrument for soil-water content measurement: sensor configurations, Soil Sci. Soc. AM. J. 51 (1987) 287–290.
[16] P.J. McDonald, B. Newling, Stray field magnetic resonance imaging, Rep. Prog. Phys. 61 (1998) 1441–1493.
[17] P.M. Glover, P.S. Aptaker, J.R. Bowler, E. Ciampi, P.J. McDonald, A Novel High-Gradient Permanent magnet for the Profiling of Planar Films and Coatings, J. Magn. Reson. 139 (1999) 90–97.
[18] R.F. Paetzold, G.A. Matzkanin, A. De Los Santos, Surface soil water content measurement using pulsed nuclear magnetic resonance technique, Soil Sci. Soc. AM. J. 49 (1985) 537–540.
[19] R.H. Varian, Ground liquid prospecting method and apparatus, US Patent 3,019,383, 1962.
[20] M. Schirov, A. Legchenko, G. Creer, A new direct non-invasive groundwater detection technology for Australia, Exploration Geophys. 22 (1991) 333–338.
[21] A. Legchenko, P. Valla, A review of basic principles for proton magnetic resonance sounding measurements, J. Appl. Geophys. 50 (2002) 3–19.
[22] A. Legchenko, J.M. Baltassat, A. Beauce, J. Bernard, Nuclear magnetic resonance as a geophysical tool for hydrogeologists, J. Appl. Geophys. 50 (2002) 21–46.
[23] M. Hertrich, M. Braun, U. Yaramanci, Magnetic Resonance Soundings with separated transmitter and receiver loops, Near Surf. Geophys. 3 (2005) 141–154.
[24] E. Fukushima, J.A. Jackson, Unilateral magnet having a remote uniform field region for nuclear magnetic resonance, US Patent 6,489,872, 2002.
[25] E. Fukushima, J.A. Jackson, Unilateral magnet having a remote uniform field region for nuclear magnetic resonance, US Patent 6,828,892, 2004.
[26] T. Munsat, W.M. Hooke, S.P. Bozeman, S. Washburn, Two new planar coil designs for a high pressure radio frequency plasma source, Appl. Phys. Lett. 66 (1995) 2180–2182.
[27] P.C. Lauterbur, Image formation by induced local interactions. Examples employing NMR, Nature 242 (1973) 190–191.
[28] J.P. Hornak, J. Szumowski, R.G. Bryant, Magnetic field mapping, Magn. Reson. Med. 6 (1988) 158–163.
[29] E.L. Hahn, Spin echoes, Phys. Rev. 77 (1950) 580–594.
[30] J.D. Gaskill, Linear Systems, Fourier Transforms, and Optics, John Wiley & Sons, NY, 1978.
[31] A.K. Jain, Fundamentals of Digital Image Processing, Prentice Hall, NJ, 1989.
[32] H.Y. Carr, E.M. Purcell, Effects of Diffusion on Free Precession in Nuclear Magnetic Resonance, Phys. Rev. 94 (1954) 630–638.
[33] S. Meiboom, D. Gill, Modified spin-echo method for measuring nuclear relaxation times, Rev. Sci. Instrum. 29 (1958) 668–691.
[34] J.P. Hornak, J.K. Moscicki, D.J. Schneider, J.H. Freed, Diffusion coefficients in anisotropic fluids by ESR imaging, J. Chem. Phys. 84 (1986) 3387–3395.
[35] Y. Geoffrion, M. Rydzy, K.W. Butler, I.C.P. Smith, H.C. Jarrell, The use of immobilized ferrite to enhance the depth selectivity of in vivo surface coil NMR spectroscopy, NMR Biomed. 1 (1988) 107–112.
[36] W. Chen, J.J.H. Ackerman, Surface coil single-pulse localization in vivo via inhomogeneous surface spoiling magnetic gradient, NMR Biomed. 4 (1989) 205–207.